Androgen Deficiency Exacerbates High-Fat Diet-Induced Metabolic Alterations in Male Mice

Vanessa Dubois, Michaël R. Laurent, Ferran Jardi, Leen Antonio, Katleen Lemaire, Lotte Goyvaerts, Louise Deldicque, Geert Carmeliet, Brigitte Decallonne, Dirk Vanderschueren, and Frank Claessens

Molecular Endocrinology Laboratory (V.D., M.R.L., L.A., F.C.), Department of Cellular and Molecular Medicine, KU Leuven, 3000 Leuven, Belgium; Gerontology and Geriatrics (M.R.L.), KU Leuven, 3000 Leuven, Belgium; Clinical and Experimental Endocrinology (F.J., L.A., G.C., B.D., D.V.), Department of Clinical and Experimental Medicine, KU Leuven, 3000 Leuven, Belgium; Gene Expression Unit (K.L., L.G.), Department of Cellular and Molecular Medicine, KU Leuven, 3000 Leuven, Belgium; Exercise Physiology Research Group (L.D.), Department of Kinesiology, KU Leuven, 3000 Leuven, Belgium; and Institute of Neuroscience (L.D.), Université Catholique de Louvain, 1348 Louvain-la-Neuve, Belgium

Androgen deficiency is associated with obesity, metabolic syndrome, and type 2 diabetes mellitus in men, but the mechanisms behind these associations remain unclear. In this study, we investigated the combined effects of androgen deficiency and high-fat diet (HFD) on body composition and glucose homeostasis in C57BL/6J male mice. Two models of androgen deficiency were used: orchidectomy (ORX) and androgen receptor knockout mice. Both models displayed higher adiposity and serum leptin levels upon HFD, whereas no differences were seen on a regular diet. Fat accumulation in HFD ORX animals was accompanied by increased sedentary behavior and occurred in spite of reduced food intake. HFD ORX mice showed white adipocyte hypertrophy, correlated with decreased mitochondrial content but not function as well as increased lipogenesis and decreased lipolysis suggested by the up-regulation of fatty acid synthase and the down-regulation of hormone-sensitive lipase. Both ORX and androgen receptor knockout exacerbated HFD-induced glucose intolerance by impairing insulin action in liver and skeletal muscle, as evidenced by the increased triglyceride and decreased glycogen content in these tissues. In addition, serum IL-1β levels were elevated, and pancreatic insulin secretion was impaired after ORX. Testosterone but not dihydrotestosterone supplementation restored the castration effects on body composition and glucose homeostasis. We conclude that sex steroid deficiency in combination with HFD exacerbates adiposity, insulin resistance, and β-cell failure in 2 preclinical male mouse models. Our findings stress the importance of a healthy diet in a clinical context of androgen deficiency and may have implications for the prevention of metabolic alterations in hypogonadal men. **(*Endocrinology* 157: 648–665, 2016)**

In recent decades, Western diets combined with reduced physical activity have led to a dramatic rise in obesity in developed countries. As a consequence, the incidence of type 2 diabetes mellitus (T2D) has substantially increased worldwide (1). The adverse metabolic consequences of obesity predisposing to T2D and cardiovascular diseases are grouped under the umbrella term "metabolic syndrome," a disorder involving increased visceral adiposity, hyperlipidemia, insulin resistance, and hypertension (2). High-fat diet (HFD) administration in rodents is the most commonly used model reproducing these metabolic adversities (3).

Abbreviations: AMPK, AMP-activated protein kinase; AR, androgen receptor; ARKO, AR knockout; AUC, area under the curve; BAT, brown adipose tissue; BW, body weight; DHT, 5α-dihydrotestosterone; FAS, fatty acid synthase; GLUT4, glucose transporter 4; HFD, high-fat diet; Hk2, hexokinase 2; HOMA-IR, homeostasis model assessment of insulin resistance; Lipe, hormone-sensitive lipase; Lpl, lipoprotein lipase; mtCo, cytochrome oxidase; ORO, Oil red O; ORX, orchidectomized; PAS, periodic acid-Schiff; PEPCK, phosphoenolpyruvate carboxykinase; Pfkm, phosphofructokinase; PTP1B, protein-tyrosine phosphatase 1B; RD, regular diet; satARKO, satellite cell-specific ARKO; SDH, succinate dehydrogenase; SHAM, sham operated; SREBP1c, sterol regulatory element-binding protein 1c; T, testosterone; T2D, type 2 diabetes mellitus; WAT, white adipose tissue; WT, wild-type.

ISSN Print 0013-7227 ISSN Online 1945-7170
Printed in USA

Received August 11, 2015. Accepted November 5, 2015.
First Published Online November 12, 2015

Androgens are steroid hormones which are, in men, secreted predominantly by the testes. The major gonadal androgen is testosterone (T). In some peripheral tissues, T is converted by 5α-reductase enzymes into the more potent androgen 5α-dihydrotestosterone (DHT), which, like T, activates the androgen receptor (AR). The AR is a ligand-inducible transcription factor that binds to specific DNA sequences to facilitate the transcription of androgen target genes (4).

With aging, bioavailable androgen concentrations decline progressively in men (5). Declining androgen levels in older men may contribute not only to sexual dysfunction and sarcopenia (5, 6) but have also been linked to metabolic disorders including T2D (7). In addition, obesity itself has been associated with decreased bioactive androgen levels (8), although it remains unclear to what extent this further aggravates obesity and T2D risk (9). Furthermore, patients receiving androgen deprivation therapy as a treatment for metastatic prostate cancer are also at increased risk for metabolic alterations such as an increase in waist circumference and a decrease in insulin sensitivity (10). Accordingly, an obese phenotype with insulin resistance has been reported in a global AR knockout (ARKO) mouse model (11). However, the exact mechanism of how androgens affect glucose homeostasis and insulin action, as well as the interaction between hypogonadism and HFD, remain unclear.

Here, we examined the phenotype of 20-week-old male wild-type mice that were either sham operated (SHAM) or orchidectomized (ORX) at 3 weeks of age, and compared animals that were switched to a HFD at 10 weeks of age with those which remained on a regular diet (RD). The rationale for castration at 3 weeks of age was to disrupt sex steroid signaling from early life on to facilitate comparison with the ARKO model, which has a developmental disruption of sex steroid signaling due to germline ablation of the AR gene (12). Both models have markedly reduced serum T levels, due to either absence or severe atrophy of the testes, respectively. In this study, we investigated the hypothesis that androgen deficiency would exacerbate HFD-induced alterations in body composition and glucose homeostasis in male mice.

Materials and Methods

Animals, diets, and experimental design

Mice were housed in standard cages and had ad libitum access to food and water. All experimental work involving animals was conducted with approval of the KU Leuven ethical committee (P078/2010).

Male C57BL/6J mice with a ubiquitous knockout of the AR (ARKO) and male C57BL/6J mice in which the AR gene was selectively ablated in muscle by means of a satellite cell-specific ARKO (satARKO) were generated as described previously (12, 13).

Wild-type male C57BL/6J mice (WT) were purchased from Janvier Labs. At 3 weeks of age, they were SHAM, ORX, or ORX and given continuous-release T (ORX+T) (Serva GmbH) or DHT (ORX+DHT) (Fluka Chemika) by sc Silastic implants (Silclear Tubing; Degania Silicone) in the cervical region (14, 15).

At 10 weeks of age, mice were switched to a HFD composed of 20 kcal% protein, 35 kcal% carbohydrate, and 45 kcal% fat (6 kcal% from soybean oil and 39 kcal% from lard) (D12451; Research Diets) or remained on a RD composed of 33 kcal% protein, 58 kcal% carbohydrate, and 9 kcal% fat (percent fatty acids: C14:0 [0.01%], C16:0 [0.47%], C16:1 [0.01%], C18:0 [0.08%], C18:1 [0.62%], C18:2 [1.80%], C18:3 [0.23%], C20:0 [0.01%], and C20:1 [0.02%]) (R/M-H; Ssniff Spezialdiäten GmbH). Body weight (BW) was recorded every 2 weeks. At 20 weeks of age, energy balance was assessed by indirect calorimetry, a glucose tolerance test was performed, and body composition was determined by whole-body dual-energy x-ray absorptiometry. Blood samples were obtained by cardiac puncture, followed by dissection of white adipose tissue (WAT) (perigonadal, sc, and perirenal fat), brown adipose tissue (BAT) (nuchal fat), liver, gastrocnemius muscle, pancreas, and seminal vesicles. Serum was obtained by centrifugation for 10 minutes at 13 000*g*.

Indirect calorimetry

Mice were individually housed in automated cages for indirect calorimetry (TSE Phenomaster Calocages) during 48 hours on a 12-hour light, 12-hour dark cycle at 22°C ambient temperature with ad libitum access to food and water. Food intake, oxygen consumption, carbon dioxide production, heat generation, and ambulatory activity were recorded over the 48-hour period, but only the last 24 hours were used for calculations. Respiratory exchange ratio and energy expenditure were calculated as described in Ref. 16. For adaption to single housing and specific drinking/feeding baskets, the mice were single housed for 7 days before actual measurements.

Glucose tolerance test

Mice were fasted overnight (16–18 h). Glucose (2.5-mg/g BW) was administered by ip injection, and blood glucose levels were followed during 2 hours using Accu-Chek Aviva glucostrips. All blood samples were obtained via tail bleeding.

Whole-body dual-energy x-ray absorptiometry

Lean and fat mass were analyzed in vivo using the PIXImus mouse densitometer (Lunar Corp) with an ultrahigh resolution (0.18 × 0.18 pixels, 1.6 line pairs/mm) and software version 1.45.

Serum measurements

Serum insulin was measured using the Ultra Sensitive Mouse Insulin ELISA kit (90080; Crystal Chem). The homeostasis model assessment of insulin resistance (HOMA-IR) was calculated as follows: HOMA-IR = fasting glucose (mg/dL) × fasting insulin (μU/mL)/405 (17). Serum leptin was assessed with the Mouse Leptin ELISA kit (90030; Crystal Chem). Serum levels of total cholesterol, high-density lipoprotein cholesterol, and trig-

Table 1. Antibody Table

Peptide/Protein Target	Antigen Sequence (if Known)	Name of Antibody	Manufacturer, Catalog Number, and/or Name of Individual Providing the Antibody	Species Raised in; Monoclonal or Polyclonal	Dilution Used
Insulin	Porcine pancreatic insulin	Polyclonal guinea pig antiinsulin	Dako, A0564	Polyclonal; guinea pig	1:100
Phospho-AMPKα (Thr172)	Synthetic peptide corresponding to residues surrounding Thr172 of human AMPKα	Phospho-AMPKα (Thr172) (40H9) rabbit mAb	Cell Signaling Technology, 2535	Monoclonal; rabbit	1:1000
AMPKα total	Synthetic peptide corresponding to the amino-terminal sequence of human AMPKα	AMPKα (23A3) rabbit mAb	Cell Signaling Technology, 2603	Monoclonal; rabbit	1:1000
Phospho-Akt (Ser473)	Synthetic phosphopeptide corresponding to residues surrounding Ser473 of mouse Akt	Phospho-Akt (Ser473) antibody	Cell Signaling Technology, 9271	Polyclonal; rabbit	1:1000
Akt total	Synthetic peptide at the carboxy-terminal sequence of human Akt	Akt (pan) (40D4) Mouse mAb	Cell Signaling Technology, 2920	Monoclonal; mouse	1:1000
SDH	Purified mitochondrial complex II of bovine origin	SDHA (2E3)	Santa Cruz Biotechnology, Inc, sc-59687	Monoclonal; mouse	1:1000
α-Tubulin	Microtubules from chicken embryo brain	Monoclonal anti-α-tubulin antibody produced in mouse	Sigma-Aldrich, T6199	Monoclonal; mouse	1:5000

lycerides were measured by colorimetry on a Roche-Hitachi Cobas 8000 c702 autoanalyzer. Low-density lipoprotein-cholesterol was calculated according to Friedewald's formula (18). Serum free fatty acids were measured using the NEFA kit from Wako Diagnostics. Cytokine levels (IL-1β, IL-6, and TNF-α) were determined in serum using a customized kit (V-PLEX Custom Mouse Cytokine; Meso Scale Diagnostics) and measured on a SECTOR Imager 2400 (Meso Scale Diagnostics). Serum adiponectin was assessed with the Mouse Adiponectin ELISA kit (80569; Crystal Chem). Total T_4 and total T_3 serum levels were determined using an electrochemiluminescent immunoassay on the Modular E immunoanalyzer (Roche Diagnostics). After acid-ethanol extraction, serum IGF-1 concentrations were measured by an in-house RIA (19) in the presence of an excess of IGF-2 (25 ng/tube).

Histology and immunohistochemistry

Subcutaneous adipose tissue cryosections (14 μm) were stained with hematoxylin and eosin. An Oil red O (ORO) staining was used to visualize neutral lipids in cryosections (7 μm) of liver and gastrocnemius muscle. After fixation for 10 minutes with 10% neutral-buffered formalin (Sigma-Aldrich), sections were washed with distilled water and incubated in 60% isopropanol for 5 minutes, followed by 5 minutes of incubation at room temperature (liver) or an overnight incubation at 32°C (gastrocnemius muscle) in isopropanol saturated with ORO reagents (Sigma-Aldrich). Next, a hematoxylin counterstaining was performed, and sections were mounted with 85% glycerol. A periodic acid-Schiff (PAS) staining was used to visualize glycogen depositions in liver and gastrocnemius muscle. Cryosections (7 μm) were incubated in distilled water, followed by 5 minutes of incubation in 0.5% periodic acid (Thermo Fisher Scientific). Sections were washed in distilled water and incubated in Schiff's reagent (Sigma-Aldrich) for 15 minutes, washed in distilled water, counterstained with hematoxylin, and mounted with DPX (distyrene, tricresyl phosphate, and xylene; Sigma-Aldrich). Insulin staining of pancreas paraffin sections (5 μm) was carried out on a Ventana Ultra staining platform (Roche). Guinea pig antiinsulin (A0564 from Dako) was used as primary antibody (60 min of incubation at 37°C, 1:100 dilution) (Table 1) and Alexa Fluor 488-conjugated donkey antiguinea pig (706-546-148 from Jackson ImmunoResearch) as secondary antibody (30 min of incubation at 37°C, 1:100 dilution). Sections were counterstained with 4′, 6′-diamino-2-phenylindole. Photographs were taken on a Zeiss Axioplan 2 microscope (Carl Zeiss). ImageJ software was used to determine adipocyte size (308 ± 35 adipocytes analyzed per animal) and pancreatic islet size (60 ± 15 islets analyzed per animal).

Islet insulin content and release

Pancreatic islets were isolated after infusion and digestion of the pancreata by collagenase P (20). Insulin secretion measurements were performed as described before (21). Briefly, size-matched islets (n = 5 per tube) were placed in glass tubes containing HEPES Krebs solution containing 0.5% BSA supplemented with 5mM (G5) or 20mM (G20) of glucose. Supernatant was collected after 1 hour incubation at 37°C. The islets were sonicated for 3 minutes after adding acid ethanol (final concentration, 75% ethanol, 0.1 N HCl, 1% Triton X-100). Insulin determination was performed using the Ultra Sensitive Mouse Insulin ELISA kit (90080; Crystal Chem).

Mitochondrial DNA content

Total DNA was extracted from organs using the GenElute Mammalian Genomic DNA Purification kit (Sigma-Aldrich), and total DNA concentration was measured with a Nanodrop 1000 (Thermo Fisher Scientific). Quantitative real-time PCR was performed on these DNA samples as described below to quantify the 16S mitochondrial gene. The mitochondrial DNA content was calculated as a ratio by dividing the amount of 16S by the total DNA concentration.

Tissue triglyceride and glycogen content

Triglyceride levels were measured in liver and gastrocnemius muscle using the Triglyceride Quantification kit (ab65336; Abcam) following the manufacturer's instructions for colorimetric assay. Glycogen content was measured in liver and gastrocne-

mius muscle as glucose residues after acid hydrolysis in freeze-dried tissue using a standard enzymatic fluorimetric assay (22).

Western immunoblotting

Subcutaneous WAT samples were homogenized in ice-cold lysis buffer containing 5mM HEPES (pH 8.5), 0.1% Triton X-100, and 1mM dithiothreitol using a Polytron mixer. Tissue homogenates were centrifuged, and the supernatants were collected. Protein concentrations were determined with the Coomassie Protein Assay Reagent according to the manufacturer's protocol (Thermo Fisher Scientific). A total of 20-μg proteins were mixed with Laemmli sample buffer and warmed for 5 minutes at 95°C. Proteins were separated by SDS-PAGE at 40 mA, then transferred on polyvinylidene fluoride membranes for 2 hours at 80 V. After blocking for 1 hour in a Tris-buffered saline plus 0.1% Tween 20 containing 5% nonfat dry milk, membranes were incubated at 4°C overnight with one of the next antibodies (Table 1): phospho-AMP-activated protein kinase (AMPK)αThr172 (2535), AMPKα total (2603), phospho-AktSer473 (9271), and Akt total (2920) (all Cell Signaling Technology) and succinate dehydrogenase (SDH) (sc-59687; Santa Cruz Biotechnology, Inc). Membranes were washed 3 times for 10 minutes in Tris-buffered saline plus 0.1% Tween 20, then incubated for 1 hour at room temperature with a secondary antibody conjugated to horseradish peroxidase. Three additional washes were done before chemiluminescence detection with the ECL-Plus Western blotting kit (Amersham Biosciences, GE Healthcare). The bands were captured with GeneSnap and quantified with ImageJ software. Phosphorylated proteins were reported to their respective total form, and SDH results were reported to α-tubulin (T6199; Sigma-Aldrich).

Citrate synthase activity analysis

The activity of the mitochondrial enzyme citrate synthase was determined fluorometrically (23).

Quantitative real-time PCR

Total RNA was extracted from organs using TRIzol reagent (Invitrogen) according to the manufacturer's protocols. After digestion with deoxyribonuclease I (Fermentas), cDNA was synthesized from 1-μg RNA using the RevertAid M-MuLV Reverse Transcriptase kit (Fermentas) and random hexamer primers (Fermentas). The PCR reaction mixtures (10 μL) contained 1× Platinum SYBR Green qPCR SuperMix-UDG (Invitrogen), 0.15μM each primer, and 50nM carboxy-X-rhodamine Reference Dye (Invitrogen). The 7500 Fast Real-Time PCR system (Applied Biosystems) was used with the Fast RT-PCR 2-step protocol (2 min at 50°C, 20 s at 95°C, and 40 cycles of 3 s at 95°C and 30 s at 60°C). The primer sequences are listed in Supplemental Table 1. All primers were designed to hybridize to different exons, and generation of single correct amplicons was checked by DNA sequencing and in melting curve assays. Gene expression values are expressed relative to the levels of hypoxanthine-guanine phosphoribosyltransferase mRNA.

Statistical analysis

Statistical analyses were performed using GraphPad Prism software (version 5.00 for Windows). χ^2 test was used for categorical variables, whereas for continuous variables, Student's t test and one-way ANOVA were used to analyze differences between 2 or more groups, respectively. Two-way ANOVA was used in experiments with more than 2 independent variables. If overall ANOVA revealed significant difference, Bonferroni's post hoc test was used to analyze differences between groups. Evolution of groups over time was analyzed with repeated measures ANOVA. All statistical tests were performed 2-tailed. Data are presented as means ± SEM, and $P < .05$ was considered statistically significant.

Results

Androgen deficiency combined with a HFD leads to increased adiposity

At the start of the experimental period, ORX mice displayed lower BW compared with SHAM animals (22.0 ± 0.3 vs 25.9 ± 0.4 g, $P < .05$) (Figure 1A). Both groups gained weight during the experimental period, and gained extra weight when fed a HFD as compared with a RD (Figure 1A and Supplemental Figure 1A). However, whereas ORX and SHAM mice showed similar weight gain upon RD (2.5 ± 0.2% vs 3.4 ± 0.2%, $P = .25$), HFD ORX gained more weight compared with HFD SHAM (14.8 ± 0.6% vs 12.5 ± 0.5%, $P < .05$). As a result, although RD ORX still had lower BW compared with RD SHAM animals at the end of the experimental period (24.1 ± 0.4 vs 28.8 ± 0.4 g, $P < .05$), the effect of castration on total BW was abolished in the HFD groups (36.0 ± 0.6 vs 37.3 ± 0.6 g, $P = .15$) (Figure 1A). Castration was effective in reducing endogenous androgen levels as evidenced by the decreased seminal vesicle weight in ORX compared with SHAM animals (Supplemental Figure 1B).

HFD administration led to a small but significant increase in lean mass, whereas fat mass increased almost 3-fold (Figure 1, B and C). As a result, the HFD groups showed an increase in fat mass % and a concomitant decrease in lean mass % compared with the RD groups (Figure 1, D and E). Although castration in RD conditions had no impact on these percentages, castration potentiated HFD-induced changes in lean and fat mass % (Figure 1, D and E). In line with their increased adiposity, leptin serum levels were higher in HFD ORX as compared with HFD SHAM mice (Figure 1F). We then assessed the contribution of the different fat pads to the increased adiposity of HFD ORX mice. The weight of both intraabdominal perigonadal and sc WAT pads was increased upon ORX when fed a HFD, whereas no castration effect was observed on perirenal WAT (Figure 1G). Nuchal BAT weight was decreased in HFD ORX compared with HFD SHAM animals (Figure 1G). In accordance with the observations

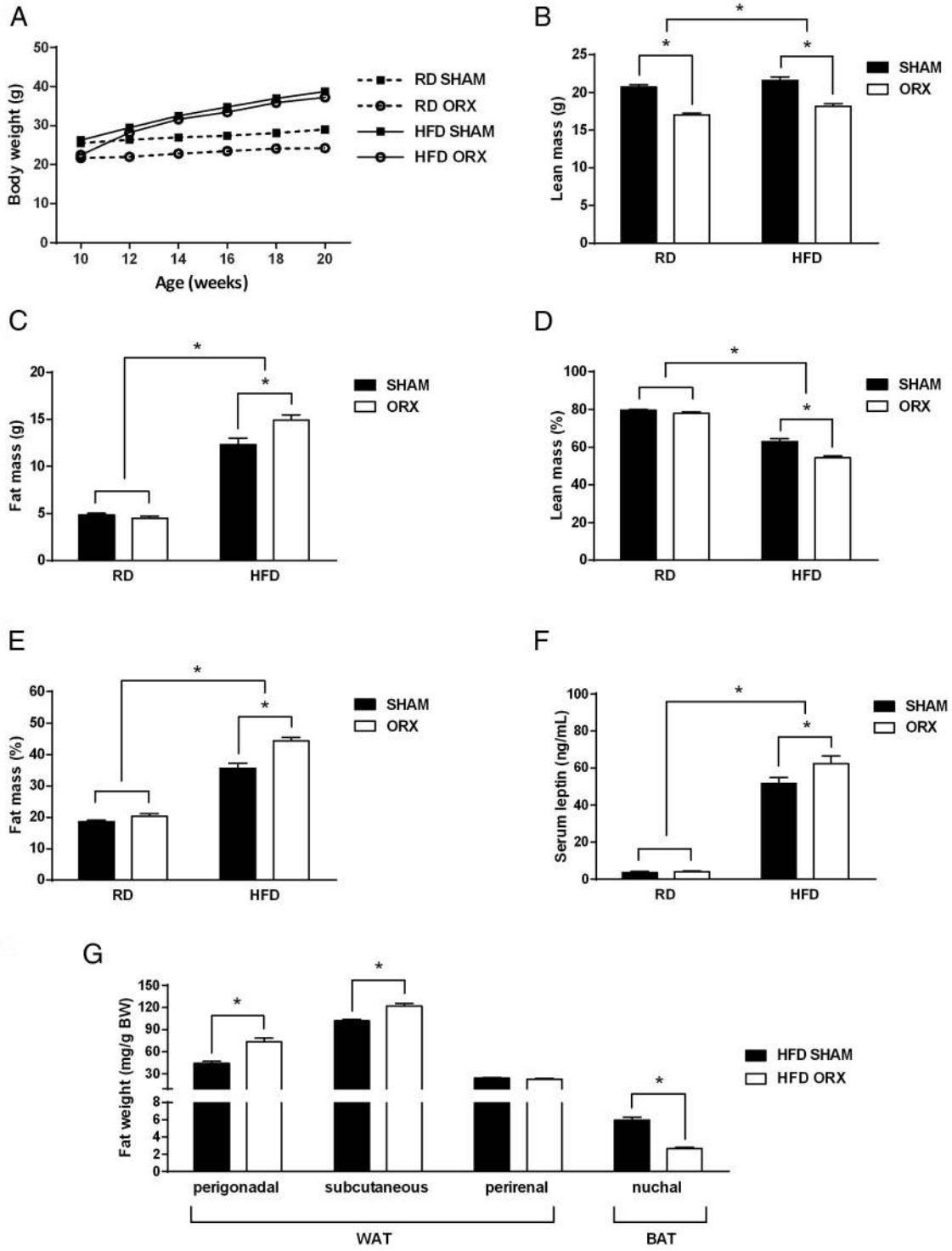

Figure 1. Effect of ORX on body composition and adiposity. A, BW of male WT mice that were SHAM or ORX at 3 weeks of age and received RD or HFD from 10 to 20 weeks of age (n = 13–15). B and C, Lean (B) and fat (C) mass of 20-week-old male WT mice that were SHAM or ORX at 3 weeks of age and received RD or HFD from 10 to 20 weeks of age, expressed in grams (n = 13–15). D and E, Lean (D) and fat (E) mass of 20-week-old male WT mice that were SHAM or ORX at 3 weeks of age and received RD or HFD from 10 to 20 weeks of age, expressed as % of BW (n = 13–15). F, Serum leptin levels of 20-week-old male WT mice that were SHAM or ORX at 3 weeks of age and received RD or HFD from 10 to 20 weeks of age (n = 10). G, Weight of different fat pads of 20-week-old male WT mice that were SHAM or ORX at 3 weeks of age and received HFD from 10 to 20 weeks of age (n = 6). Error bars indicate SEM; *, $P < .05$.

after castration, genetic AR disruption also induced a shift in body composition towards more fat when combined with a HFD (Figure 2, A–E). In addition, the rise in serum leptin observed upon HFD was more pronounced in HFD ARKO compared with HFD WT (Figure 2F). Subcutaneous WAT was increased in HFD ARKO (Figure 2G).

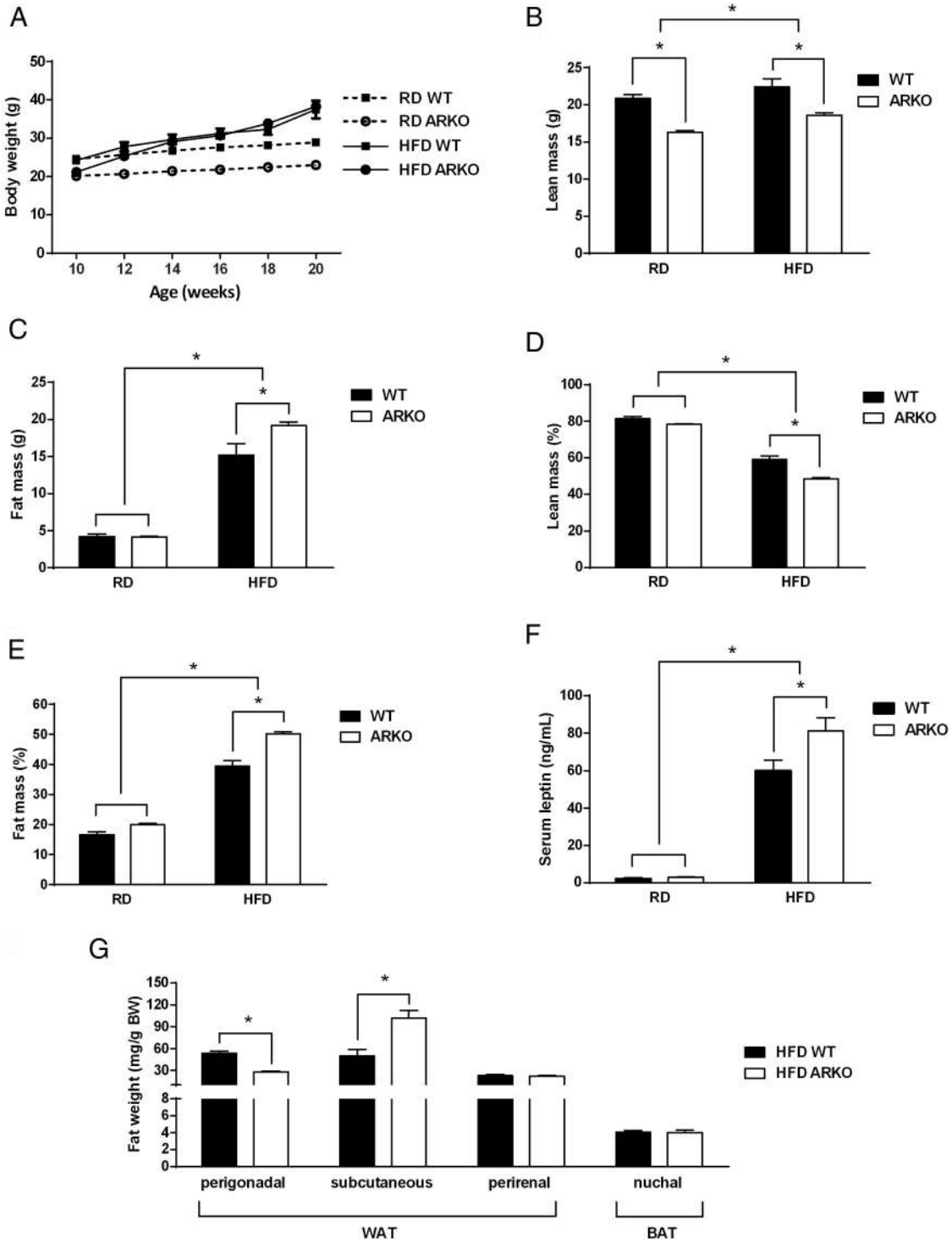

Figure 2. Effect of global AR deletion on body composition and adiposity. A, BW of 20-week-old male WT and ARKO mice that received RD or HFD from 10 to 20 weeks of age (n = 7–8). B and C, Lean (B) and fat (C) mass of 20-week-old male WT and ARKO mice that received RD or HFD from 10 to 20 weeks of age, expressed in grams (n = 7–8). D and E, Lean (D) and fat (E) mass of 20-week-old male WT and ARKO mice that received RD or HFD from 10 to 20 weeks of age, expressed as % of BW (n = 7–8). F, Serum leptin levels of 20-week-old male WT and ARKO mice that received RD or HFD from 10 to 20 weeks of age (n = 7–8). G, Weight of different fat pads of 20-week-old male WT and ARKO mice that received HFD from 10 to 20 weeks of age (n = 7–8). Error bars indicate SEM; *, $P < .05$.

However, in contrast to the ORX data, global AR deletion had no effect on BAT weight and caused a reduction in perigonadal fat mass (Figure 2G). In summary, when combined with a HFD, both castration and global AR deletion lead to increased adiposity accompanied by higher serum leptin levels.

Mechanisms underlying the increased adiposity in androgen-deficient animals receiving a HFD

Reduced ambulatory activity may have contributed to the increased adiposity observed in HFD ORX mice (Figure 3A), which occurred in spite of a significantly lower food intake (Figure 3B). HFD administration reduced the respiratory exchange ratio (Figure 3C), and increased heat generation (Figure 3D), oxygen consumption (Figure 3E) as well as energy expenditure (Figure 3F). However, these parameters were similar in HFD SHAM and HFD ORX mice (Figure 3, C–F), as were the serum levels of the thyroid hormones T_3 and T_4 and the BAT mRNA levels of uncoupling protein 1 (Supplemental Figure 2).

Histological analysis of sc WAT revealed an increase in mean adipocyte size (Figure 4, A and B), with a shift in area distribution towards larger adipocytes ($P < .0001$, χ^2 test) in HFD ORX compared with HFD SHAM mice (Figure 4C). To determine the molecular mechanisms underlying the adipocyte hypertrophy observed upon combination of androgen deficiency and HFD, we measured the expression of the lipogenic genes peroxisome proliferator-activated receptor-γ, CCAAT/enhancer-binding protein-α, sterol regulatory element-binding protein 1c (SREBP1c), adipocyte protein 2, fatty acid synthase (FAS), and acetyl-coenzyme A carboxylase, and of the lipolytic genes hormone-sensitive lipase (Lipe) and lipoprotein lipase (Lpl). The increased adiposity in HFD ORX mice was correlated with both increased lipogenesis and decreased lipolysis, as indicated by the up-regulation of FAS and the down-regulation of Lipe in HFD ORX mice compared with HFD SHAM (Figure 4D). In line with these gene expression data, levels of phosphorylated AMPK, an inhibitor of adipocyte lipolysis (24), were increased in sc WAT of HFD ORX compared with HFD SHAM (Figure 4, E and F). Levels of phosphorylated Akt were similar in both groups (Figure 4, E and G).

Mitochondria of WAT are involved in the regulation of both lipogenesis and lipolysis (25). Moreover, markers of mitochondrial biogenesis and metabolism are lower in overweight and obese subjects (26). We therefore addressed the possible contribution of mitochondrial dysfunction to the increased adiposity of HFD ORX mice. Mitochondrial DNA content was decreased in sc WAT of HFD ORX compared with HFD SHAM animals (Figure 4H). In addition, HFD ORX mice showed lower expression levels of nicotinamide adenine dinucleotide dehydrogenase 1 (mtNd1), a subunit of complex I of the mitochondrial electron transport chain (Figure 4I). Levels of cytochrome oxidase 1 (mtCo1) and cytochrome oxidase 2 (mtCo2), 2 subunits of complex IV, were not affected by ORX (Figure 4I). Activity of the mitochondrial enzyme citrate synthase was similar in sc WAT of HFD SHAM and HFD ORX mice (Figure 4J), as were the protein levels of another mitochondrial enzyme, SDH (Figure 4, K and L).

Androgen deficiency augments HFD-induced glucose intolerance

Castration had no impact on glucose tolerance in RD conditions, and glucose tolerance decreased in SHAM as well as ORX mice upon HFD (Figure 5A). In line with the increase in adiposity, castration combined with HFD induced an even more pronounced glucose intolerance, as indicated by the augmented glucose area under the curve (AUC) in HFD ORX compared with HFD SHAM mice (Figure 5A, right panel). In accordance with the castration data, AR loss exacerbated the effect of HFD on glucose tolerance (Figure 5B).

Although the decreased glucose tolerance in HFD ORX mice compared with HFD SHAM was not accompanied by significant changes in either glycemia (Figure 5C) or insulinemia (Figure 5D), there was a trend towards a higher insulin resistance index (HOMA-IR) in HFD ORX mice ($P = .07$) (Figure 5E). Accordingly, despite the absence of hyperglycemia (Figure 5F) and hyperinsulinemia (Figure 5G), HFD ARKO mice showed an increase in HOMA-IR as compared with their WT littermates (Figure 5H).

Thus, both hypogonadism models show that androgen deficiency potentiates HFD-induced glucose intolerance, likely via an impairment of insulin action.

A dual phenotype of peripheral insulin resistance and pancreatic β-cell failure

To confirm the hypothesis of impaired insulin action in androgen-deficient HFD-fed animals, we focused on 2 key target organs of insulin, ie, skeletal muscle and liver. Increased ORO staining, reflecting increased abundance of neutral lipids, was observed in liver and muscle of HFD ORX mice (Figure 6A), a finding that was mirrored by quantitative assessment of tissue lipid content (Figure 6B). Hepatic transcript levels of the lipogenic genes SREBP1c and FAS were elevated in HFD ORX (Supplemental Figure 3A). Serum lipids were however similar in HFD ORX and HFD SHAM animals (Supplemental Table 2). As evidenced by a PAS staining shown in Figure 6C, both liver and muscle glycogen content were decreased in HFD ORX mice compared with HFD SHAM, an observation that

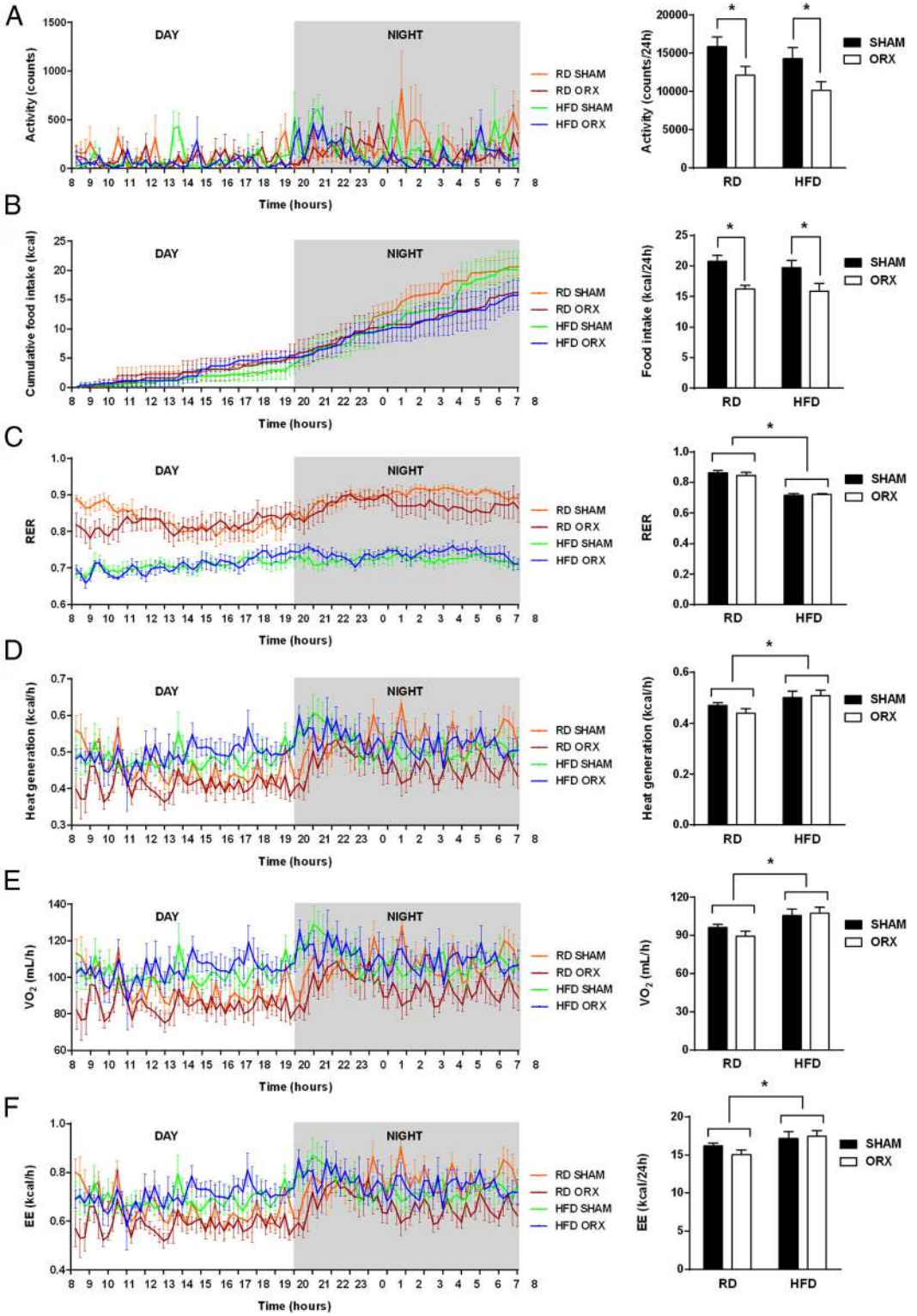

Figure 3. Effect of ORX on energy balance. Ambulatory activity (A), food intake (B), respiratory exchange ratio (RER) (C), heat generation (D), oxygen consumption (VO_2) (E), and energy expenditure (EE) (F) of 20-week-old male WT mice that were SHAM or ORX at 3 weeks of age and received RD or HFD from 10 to 20 weeks of age (n = 5–8). Left panels, Time course over the 24-hour period. Right panels, Average over the 24-hour period. Error bars indicate SEM; *, $P < .05$.

was confirmed by biochemical analysis of tissue glycogen content (Figure 6D). The decreased glycogen levels in HFD ORX mice correlated with decreased glycogen synthase expression in muscle but not liver (Supplemental Figure 3, B and C). Increased expression of the gluconeogenic enzyme phosphoenolpyruvate carboxykinase (PEPCK) as

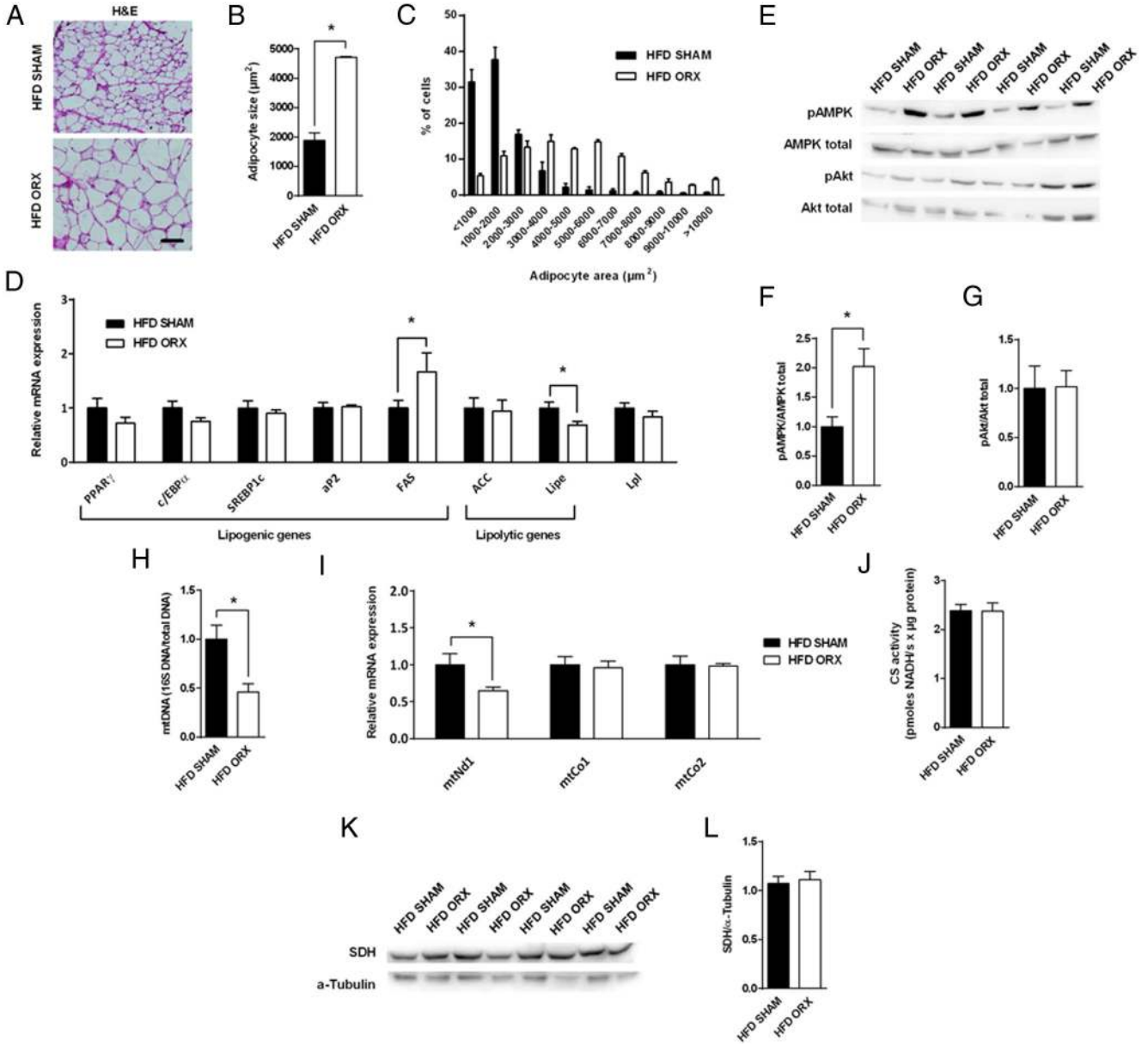

Figure 4. Effect of ORX on adipocytic cell size and area distribution, gene expression, and mitochondria. A, Hematoxylin and eosin (H&E) staining of sc WAT of 20-week-old male WT mice that were SHAM or ORX at 3 weeks of age and received HFD from 10 to 20 weeks of age. Scale bar, 100 μm. B and C, Mean adipocyte size (B) and adipocyte area distribution (C) in sc WAT of 20-week-old male WT mice that were SHAM or ORX at 3 weeks of age and received HFD from 10 to 20 weeks of age (n = 3). Notice the shift in area distribution towards larger adipocytes ($P < .0001$, χ^2 test) in HFD ORX compared with HFD SHAM mice. D, Quantitative real-time PCR analysis of mRNA levels of 6 lipogenic (peroxisome proliferator-activated receptor [PPAR]γ, CCAAT/enhancer-binding protein [c/EBP]α, SREBP1c, adipocyte protein 2 [aP2], FAS, and acetyl-coenzyme A carboxylase [ACC]) and 2 lipolytic (Lipe and Lpl) genes in sc WAT of 20-week-old male WT mice that were SHAM or ORX at 3 weeks of age and received HFD from 10 to 20 weeks of age (n = 8). E–G, Total protein extracts (20 μg) from sc WAT of 20-week-old male WT mice that were SHAM or ORX at 3 weeks of age and received HFD from 10 to 20 weeks of age were subjected to immunoblotting with antiphosphorylated AMPK, antitotal AMPK, antiphosphorylated Akt, and antitotal Akt antibodies. Representative images (E), densitometric data of phosphorylated AMPK content expressed as ratio of pAMPK to total AMPK (n = 9) (F), and densitometric data of phosphorylated Akt content expressed as ratio of pAkt to total Akt (n = 9) (G) are shown. H, Mitochondrial (mt) DNA content in sc WAT of 20-week-old male WT mice that were SHAM or ORX at 3 weeks of age and received HFD from 10 to 20 weeks of age (n = 8). I, Quantitative real-time PCR analysis of mRNA levels of 3 mitochondrial genes (mtNd1, mtCo1, and mtCo2) in sc WAT of 20-week-old male WT mice that were SHAM or ORX at 3 weeks of age and received HFD from 10 to 20 weeks of age (n = 8). J, Activity of the mitochondrial enzyme citrate synthase (CS) in total protein extracts (2 μg) from sc WAT of 20-week-old male WT mice that were SHAM or ORX at 3 weeks of age and received HFD from 10 to 20 weeks of age (n = 10). K and L, Total protein extracts (20 μg) from sc WAT of 20-week-old male WT mice that were SHAM or ORX at 3 weeks of age and received HFD from 10 to 20 weeks of age were subjected to immunoblotting with an antibody against the mitochondrial enzyme SDH. As a loading control, α-tubulin was used. Representative image (K) and densitometric data of SDH content expressed as ratio of SDH to α-tubulin (n = 8–9) (L) are shown. Error bars indicate SEM; *, $P < .05$.

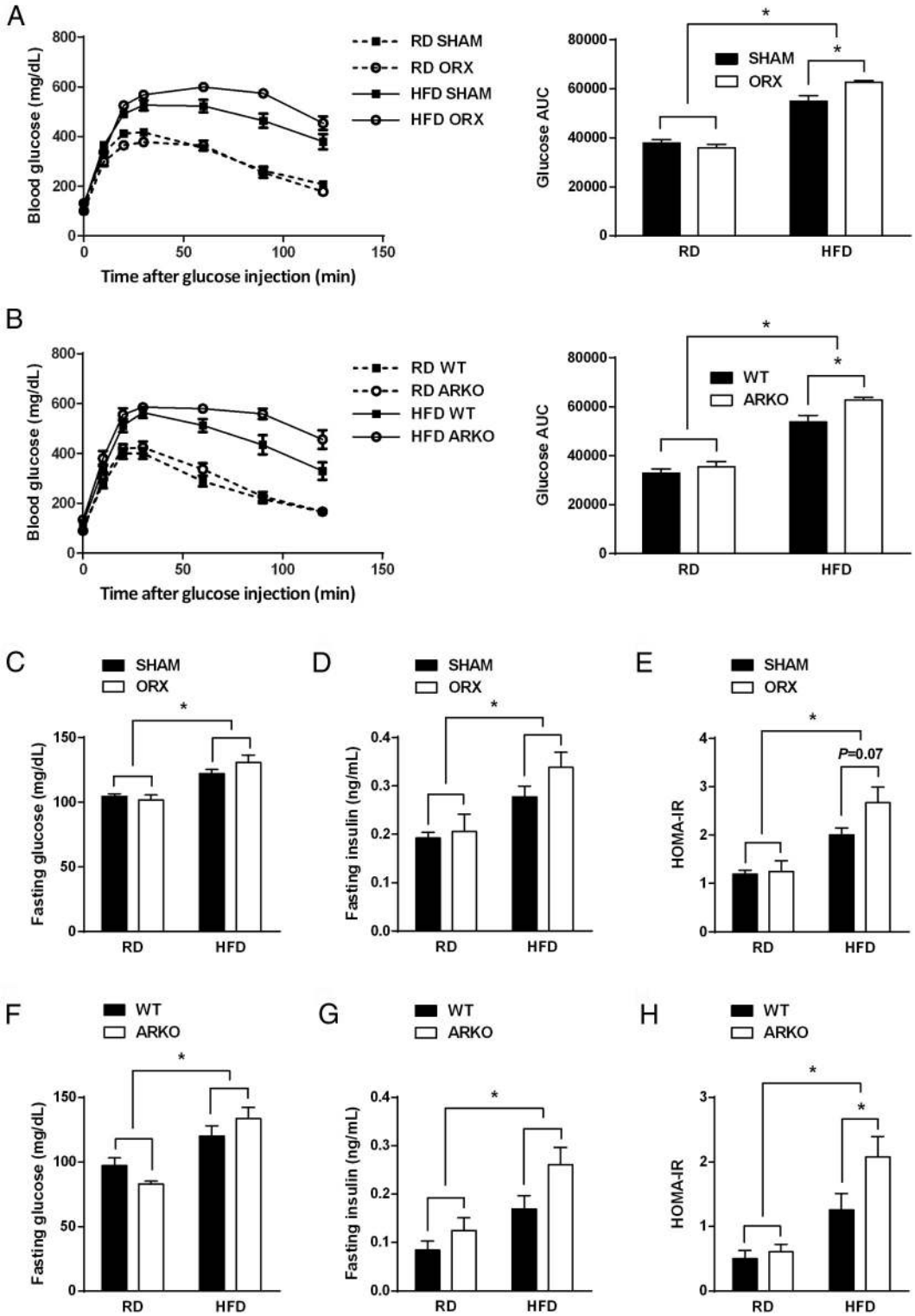

Figure 5. Effect of ORX and global AR deletion on glucose tolerance. A, left panel, After a 16- to 18-hour fast, 20-week-old male WT mice that were SHAM or ORX at 3 weeks of age and received RD or HFD from 10 to 20 weeks of age were injected ip with 2.5-mg/g BW glucose. Blood glucose was monitored for 2 hours (n = 13–15). Right panel, AUC was calculated for the curves of the left panel. B, left panel, After a 16- to 18-hour fast, 20-week-old male WT and ARKO mice that received RD or HFD from 10 to 20 weeks of age were injected ip with 2.5-mg/g BW glucose. Blood glucose was monitored for 2 hours (n = 7–8). Right panel, AUC was calculated for the curves of the left panel. C–E, After a 16- to 18-hour fast, blood glucose (C) and serum insulin (D) were determined, and HOMA-IR (E) was calculated of 20-week-old male WT mice that were SHAM or ORX at 3 weeks of age and received RD or HFD from 10 to 20 weeks of age (n = 10). F–H, After a 16- to 18-hour fast, blood glucose (F) and serum insulin (G) were determined, and HOMA-IR (H) was calculated of 20-week-old male WT and ARKO mice that received RD or HFD from 10 to 20 weeks of age (n = 7–8). Error bars indicate SEM; *, $P < .05$.

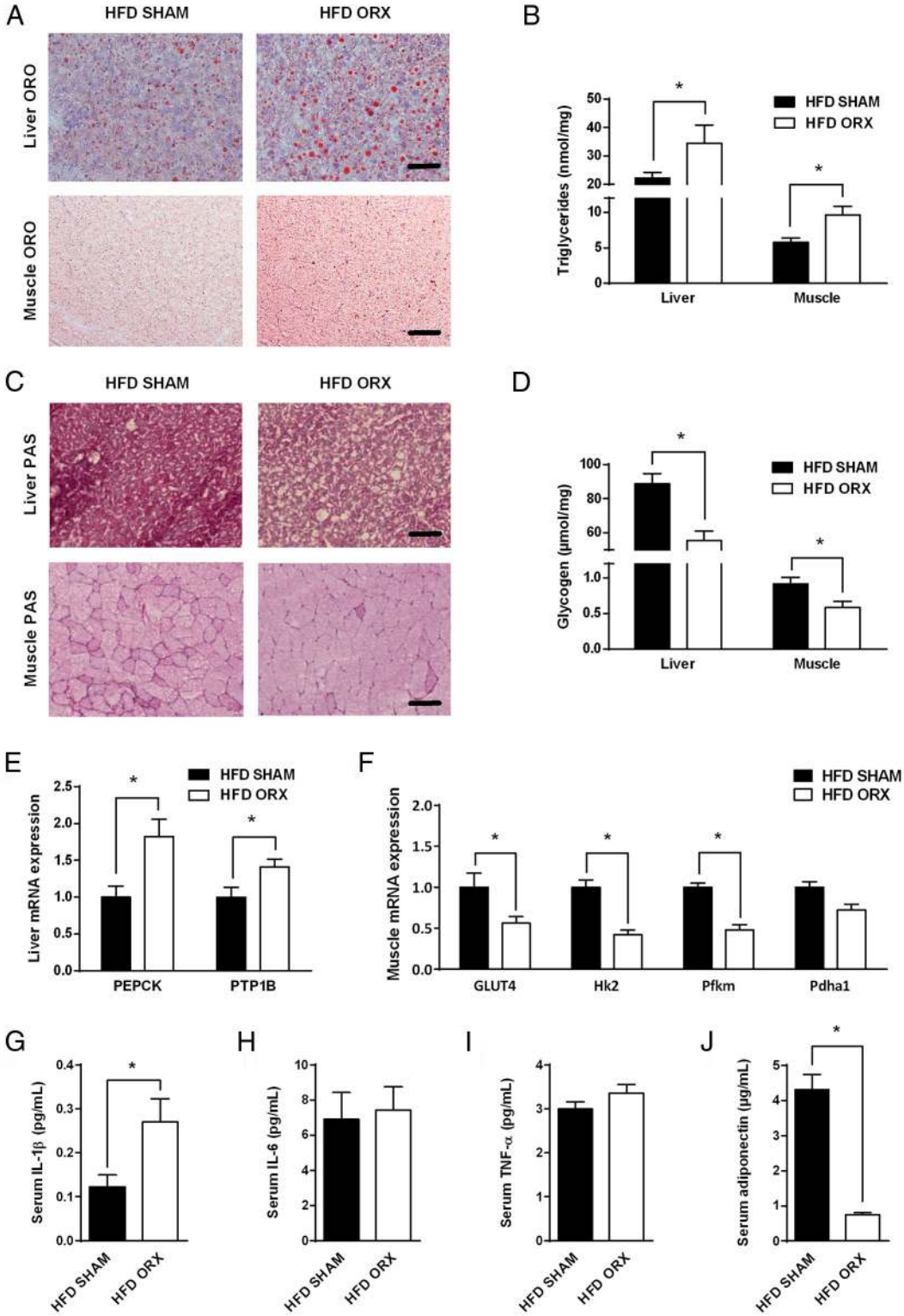

Figure 6. Effect of ORX on peripheral insulin sensitivity. A–D, ORO staining (A), triglyceride content (B), PAS staining (C), and glycogen content (D) of liver and gastrocnemius muscle of 20-week-old male WT mice that were SHAM or ORX at 3 weeks of age and received HFD from 10 to 20 weeks of age (n = 10–12). Scale bar, 50 μm (liver) or 100 μm (muscle). E and F, Quantitative real-time PCR analysis of mRNA levels of PEPCK and PTP1B in liver (E) and of GLUT4, Hk2, Pfkm, and Pdha1 in gastrocnemius muscle (F) of 20-week-old male WT mice that were SHAM or ORX at 3 weeks of age and received HFD from 10 to 20 weeks of age (n = 8). G–J, Serum levels of IL-1β (G), IL-6 (H), TNF-α (I), and adiponectin (J) of 20-week-old male WT mice that were SHAM or ORX at 3 weeks of age and received HFD from 10 to 20 weeks of age (n = 9). Error bars indicate SEM; *, $P < .05$.

well as of protein-tyrosine phosphatase 1B (PTP1B), a negative regulator of insulin signaling, in liver of HFD ORX mice further confirmed hepatic insulin resistance (Figure 6E). PEPCK and PTP1B were also up-regulated in liver from HFD ARKO animals compared with HFD WT littermates (Supplemental Figure 4A). Muscular insulin resistance was further confirmed by analyzing the expression of several key regulators of glucose uptake and use in muscle. Decreased expression of glucose transporter 4 (GLUT4), hexokinase 2 (Hk2), and phosphofructokinase (Pfkm), genes involved in glucose uptake and its commitment to the glycolytic pathway, was observed in HFD ORX mice compared with HFD SHAM (Figure 6F). These genes were also down-regulated in muscle from HFD ARKO animals compared with HFD WT littermates (Supplemental Figure 4B). Levels of pyruvate dehydrogenase E1-α1 (Pdha1), a gene involved in the link between glycolysis and the Krebs cycle, were not affected (Figure 6F). To determine the contribution of muscle AR to the metabolic phenotype we observed in androgen-deficient HFD-fed animals, we studied a mouse model in which the AR gene was selectively ablated in muscle by means of a satARKO (13). Loss of AR signaling in muscle was not sufficient to potentiate the HFD-induced metabolic alterations, as evidenced by the similar body composition and glucose tolerance of HFD-fed satARKO mice compared with their control littermates (Supplemental Figure 5). Finally, we measured proinflammatory cytokines in the serum of HFD SHAM and HFD ORX mice, because chronic low-grade inflammation is described to play a key role in the pathogenesis of peripheral insulin resistance (27). Levels of IL-1β were increased in HFD ORX compared with the SHAM controls (Figure 6G). Serum concentrations of IL-6 and TNF-α were similar in both groups (Figure 6, H and I). In line with their reduced insulin sensitivity, HFD ORX mice displayed strongly decreased circulating levels of adiponectin (Figure 6J).

Insulin secretion in response to a glucose challenge was markedly reduced in HFD ORX mice as compared with HFD SHAM (Figure 7A), suggesting that androgen deficiency combined with HFD leads to the typical dual phenotype of peripheral insulin resistance and failure of the pancreatic β-cells to compensate this resistance by increasing insulin secretion. This was further confirmed by a decrease in insulin secretion after glucose injection in HFD ARKO mice compared with their WT littermates (Figure 7B). To visualize the islets of Langerhans, insulin staining was performed on pancreas sections (Figure 7C). Total number of islets was similar in HFD SHAM and HFD ORX mice (Figure 7D), as were mean islet size and area distribution (Figure 7, E and F).

To investigate whether this pancreatic β-cell failure is an indirect consequence of the peripheral insulin resistance or a direct castration effect, we measured insulin content and release in pancreatic islets isolated from RD SHAM and RD ORX mice, which do not show metabolic alterations. Glucose-stimulated insulin secretion was similar in RD SHAM and RD ORX animals (Figure 7G), as was the islet insulin content (Figure 7H).

T but not DHT supplementation restores the castration effects on body composition and glucose homeostasis

We next aimed to examine the effects of the endogenous androgens T and DHT on body composition and glucose metabolism. To this end, we castrated 2 additional groups of WT mice, supplemented them with either T (ORX+T) or DHT (ORX+DHT), and fed them a HFD. Hormone replacement was effective, as indicated by the restoration of seminal vesicle weight to SHAM levels in ORX+T and ORX+DHT mice (Supplemental Figure 6). Although T supplementation restored lean and fat mass to SHAM levels, DHT supplementation failed to reverse the decrease in lean mass and the increase in fat mass observed in HFD ORX mice compared with HFD SHAM (Figure 8, A–C). Accordingly, the increase in serum leptin perceived upon ORX was abolished by T but not DHT (Figure 8D). In contrast to ORX+T animals, ORX+DHT mice also showed augmented glucose intolerance and decreased compensatory insulin secretion compared with the SHAM group, similar to ORX mice (Figure 8, E and F). T as well as DHT abolished the increase in hepatic PEPCK expression perceived upon ORX (Figure 8G). The ORX-associated decreases in muscular GLUT4, Hk2, and Pfkm transcript levels were, however, rescued by T but not DHT (Figure 8H). The differential effects of T and DHT could not be attributed to differences in circulating IGF-1 (Supplemental Figure 7).

Discussion

Sex steroid deficiency in men is associated with obesity, metabolic syndrome, and T2D (7, 28), but the underlying causality and mechanisms remain unclear. On the one hand, men with acquired hypogonadism develop increased fat mass (29), and T replacement in hypogonadal men reduces fat mass (30). On the other hand, low T may be a consequence rather than the cause of obesity. Indeed, surveys in aging men reveal that obesity is strongly associated with low T but also low LH levels, reflecting hypothalamic-pituitary-gonadal axis dysfunction or second-

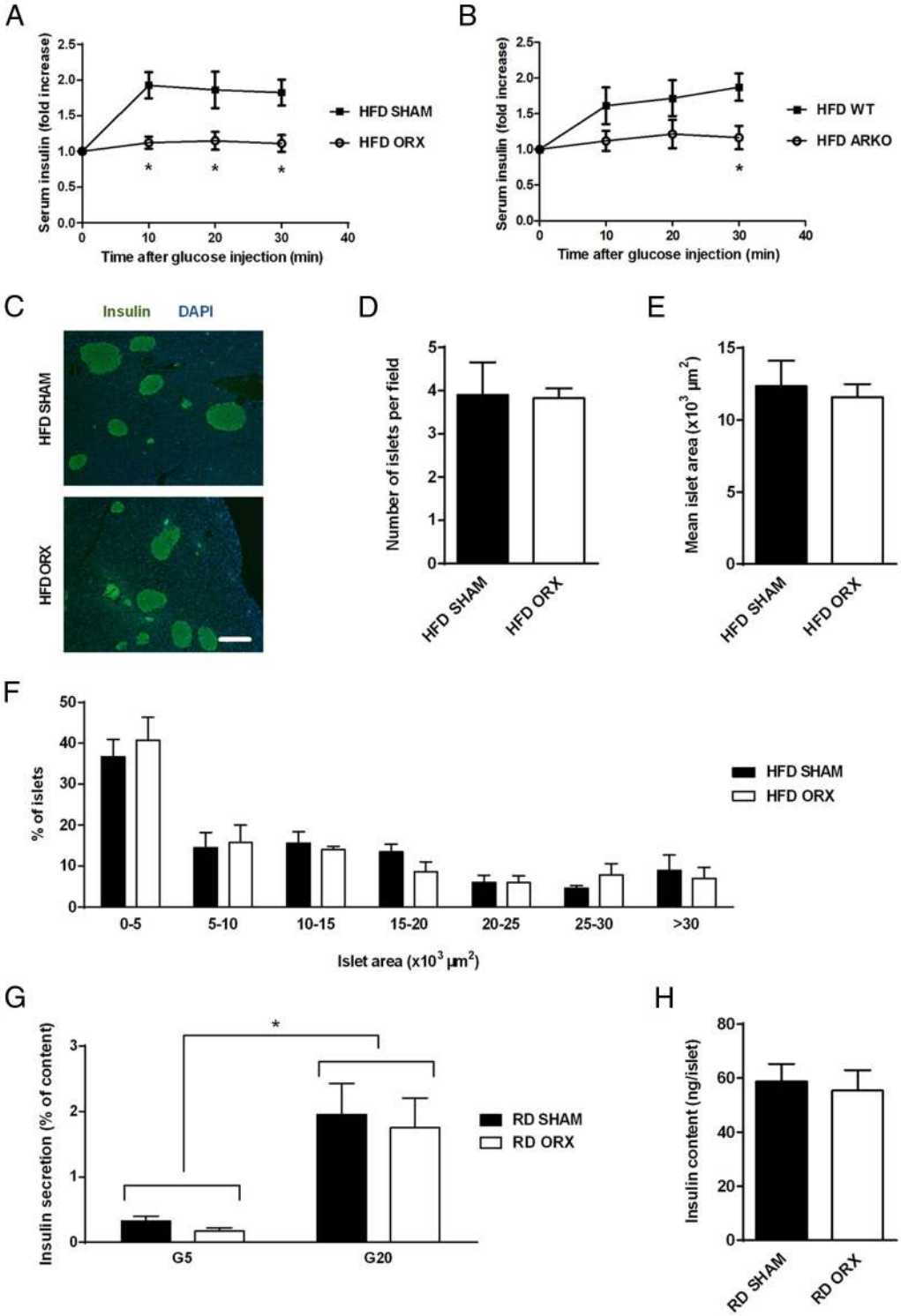

Figure 7. Effect of ORX and global AR deletion on glucose-stimulated insulin secretion and pancreatic islets. A, After a 16- to 18-hour fast, 20-week-old male WT mice that were SHAM or ORX at 3 weeks of age and received HFD from 10 to 20 weeks of age were injected ip with 2.5-mg/g BW glucose. Serum insulin was monitored for 30 minutes (n = 10). B, After a 16- to 18-hour fast, 20-week-old male WT and ARKO mice that received HFD from 10 to 20 weeks of age were injected ip with 2.5-mg/g BW glucose. Serum insulin was monitored for 30 minutes (n = 7–8). C, Pancreas sections 20-week-old male WT mice that were SHAM or ORX at 3 weeks of age and received HFD from 10 to 20 weeks of age were stained for insulin (green) and 4′, 6′-diamino-2-phenylindole (blue). Scale bar, 200 μm. D–F, Number of islets (D), mean islet area (E), and islet area distribution (F) in pancreas of 20-week-old male WT mice that were SHAM or ORX at 3 weeks of age and received HFD from 10 to 20 weeks of age (n = 3). G and H, Islets from 20-week-old male WT mice that were SHAM or ORX at 3 weeks of age and received RD from 10 to 20 weeks of age were isolated and incubated for 1 hour with 5mM (G5) or 20mM (G20) of glucose. Insulin release (G) was quantified as the percentage of insulin secreted compared with islet insulin content (H) (n = 4). Error bars indicate SEM; *, $P < .05$.

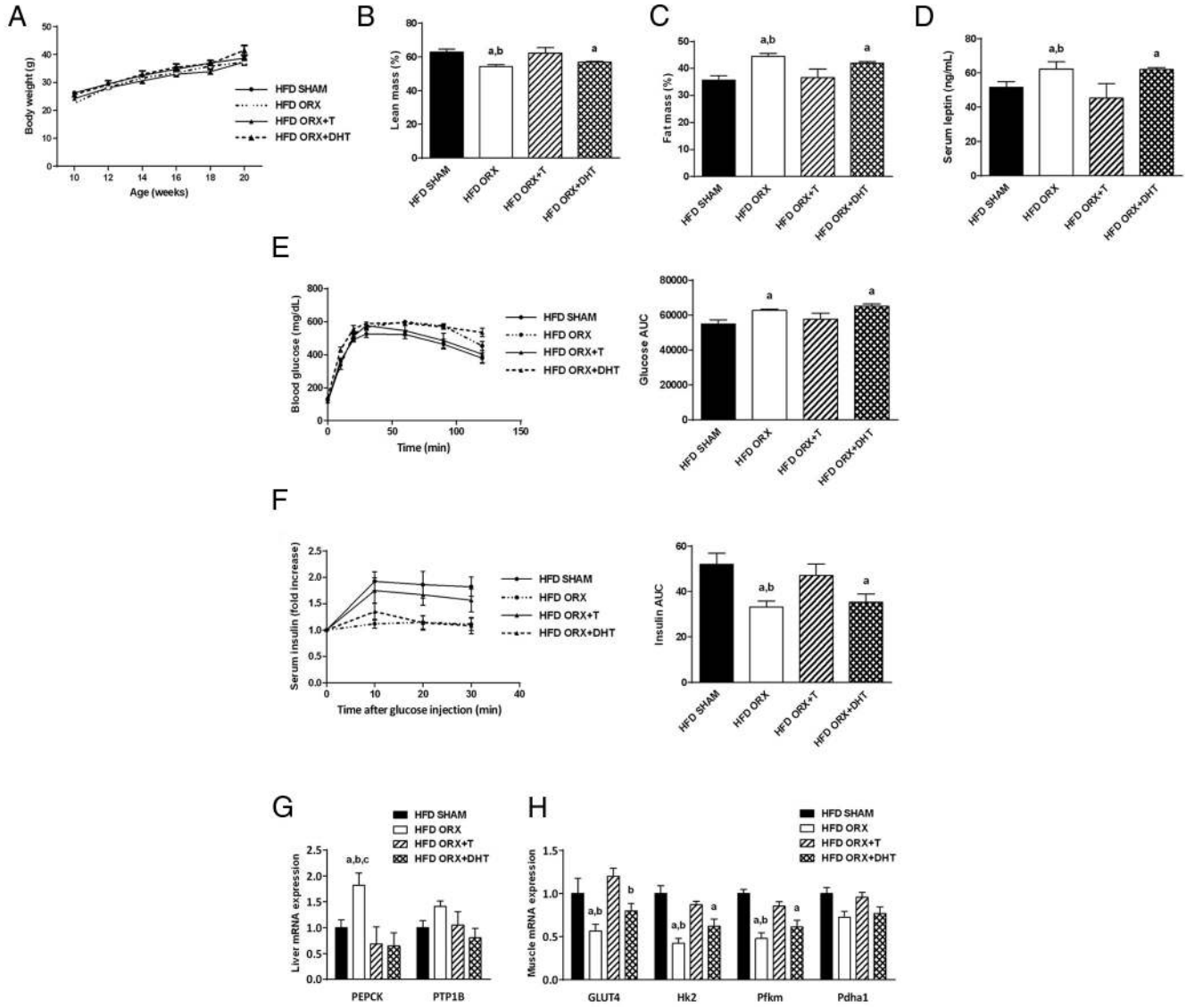

Figure 8. Effect of T and DHT supplementation on metabolic phenotype. A, BW of male WT mice that were SHAM, ORX, or ORX and treated with T (ORX+T) or DHT (ORX+DHT) at 3 weeks of age and received HFD from 10 to 20 weeks of age (n = 5–8). B and C, Lean (B) and fat (C) mass expressed as % of BW of 20-week-old male WT mice that were SHAM, ORX, ORX+T, or ORX+DHT at 3 weeks of age and received HFD from 10 to 20 weeks of age (n = 5–8). D, Serum leptin levels of 20-week-old male WT mice that were SHAM, ORX, ORX+T, or ORX+DHT at 3 weeks of age and received HFD from 10 to 20 weeks of age (n = 5–8). E, left panel, After a 16- to 18-hour fast, 20-week-old male WT mice that were SHAM, ORX, ORX+T, or ORX+DHT at 3 weeks of age and received HFD from 10 to 20 weeks of age were injected ip with 2.5-mg/g BW glucose. Blood glucose was monitored for 2 hours (n = 5–8). Right panel, AUC was calculated for the curves of the left panel. F, left panel, After a 16- to 18-hour fast, 20-week-old male WT mice that were SHAM, ORX, ORX+T, or ORX+DHT at 3 weeks of age and received HFD from 10 to 20 weeks of age were injected ip with 2.5-mg/g BW glucose. Serum insulin was monitored for 30 minutes (n = 5–8). Right panel, AUC was calculated for the curves of the left panel. G and H, Quantitative real-time PCR analysis of mRNA levels of PEPCK and PTP1B in liver (G) and of GLUT4, Hk2, Pfkm, and Pdha1 in gastrocnemius muscle (H) of 20-week-old male WT mice that were SHAM, ORX, ORX+T, or ORX+DHT at 3 weeks of age and received HFD from 10 to 20 weeks of age (n = 5–8). Error bars indicate SEM; a, $P < .05$ compared with HFD SHAM; b, $P < .05$ compared with HFD ORX+T; c, $P < .05$ compared with HFD ORX+DHT.

ary hypogonadism (31, 32). Weight loss reversed the low T levels observed in severely obese men (33).

In the present study, we therefore examined the combined effect of androgen deficiency and HFD on body composition and glucose homeostasis in 2 rodent models of hypogonadism, ie, ORX and global AR deletion (ARKO). Establishment of androgen deficiency from early life on as well as developmental disruption of AR signaling did not result in metabolic abnormalities in RD conditions, but led to increased susceptibility to HFD-induced adiposity and glucose intolerance at adult age. Importantly, seminal vesicle weight was also decreased in obese eugonadal animals (HFD SHAM) compared with lean controls (RD SHAM) (Supplemental Figure 1B), indicating that the relationship between obesity and T is likely bidirectional. There are numerous reports of mouse mod-

els which only display phenotypic abnormalities in the presence of an additional challenge, like in this case a HFD. For example, male mice with hepatic AR ablation exhibit only moderate liver steatosis when fed a standard chow diet, but develop obesity, glucose intolerance, and insulin resistance when fed a HFD (34). Similarly, mice which lack one allele of eukaryotic translation initiation factor 2A, a gene important for translation initiation, show β-cell failure and type 2 diabetes but only when stressed by a HFD (35). The need of experimental challenge to expose underlying phenotypes is likely due to compensation mechanisms of the body, which tries to accommodate for example androgen loss but fails to remain in balance when an environmental triggering factor such as HFD is added.

Three other models of global AR deletion generated by others already show increased adiposity when fed standard chow (11, 36, 37). In contrast to these models, the global ARKO developed by our group (12) showed no increased adiposity when fed a standard diet (38), a finding that was confirmed in this study. The reason for the discrepancy in adiposity between the models remains currently unknown. However, it should be noted that, although the first 3 models show an obese phenotype at advanced age, phenotyping of our ARKO model was performed earlier. Therefore, development of late-onset obesity with standard chow cannot be excluded.

Sexual dimorphism in adipose tissue distribution, with men carrying more intraabdominal fat compared with women, has been proposed to be an important factor in explaining the gender differences in metabolic risk profile (39). However, a role for sex steroids in the regulation of fat distribution is controversial, because hypogonadism seems to increase adiposity in men irrespective of fat localization (40). Subcutaneous fat mass was augmented in both ORX and ARKO mice fed a HFD. Although intraabdominal perigonadal fat was also increased in ORX HFD-fed animals, HFD ARKO mice showed diminished perigonadal fat mass compared with their WT littermates. This is most likely linked to the impaired development of the internal reproductive tract in ARKO mice (37). Subcutaneous fat is indeed the most androgen-responsive fat pad in rodents (41), and our histological analysis revealed an increase in adipocyte size. Also in obese subjects, fat accumulation is mostly due to adipocyte hypertrophy rather than increased adipocyte number (42). To further investigate the molecular mechanisms underlying the increased adiposity in androgen-deficient HFD-fed mice, we measured the levels of lipogenic and lipolytic genes. The up-regulation of FAS and the down-regulation of Lipe in sc fat of HFD ORX compared with HFD SHAM mice indicates that the increased adiposity is due to both increased lipogenesis and decreased lipolysis. These findings strengthen earlier studies that describe a role of androgens in lipogenesis (11) and lipolysis (36) in more detail.

We and others observed earlier that ORX as well as global AR deletion induces a reduction in voluntary (37, 38, 43) as well as spontaneous (36) activity. It is most likely that the impact of loss of androgen signaling on motivation for physical exercise may have contributed to the increase in adiposity which we observed in this study. On the other hand, the hypophagic effect of androgen deficiency is also well documented (44). Despite a decrease in food intake, we observed an additive increase in adiposity in HFD ORX mice. It is tempting to speculate that the decrease in food intake may be a secondary consequence of decreased physical activity. However, it is also possible that there is a direct androgen regulation of food intake (44). We found no evidence that androgens influence obesity-induced metabolic dysregulation via heat generation or energy expenditure.

Both ORX and global AR deletion exacerbated glucose intolerance in the HFD-fed groups. When compared with the SHAM and WT controls, the glucose intolerance in ORX and ARKO HFD-fed mice was not accompanied by hyperglycemia or hyperinsulinemia. However, although not significant, serum insulin tended to be higher in the androgen-deficient HFD-fed mice in both models, pointing towards insulin resistance. In addition, the HOMA-IR index was increased in HFD ARKO. Thus, our data suggest that androgen deficiency potentiates the HFD-induced glucose intolerance via an impairment of insulin action. The latter was confirmed by the increased triglyceride and lowered glycogen content in skeletal muscle and liver observed by us and others (45–47). Increased expression of PEPCK, a key regulator of hepatic gluconeogenesis which is suppressed by insulin, in liver of HFD ORX mice further evidenced the hepatic insulin resistance. Muscular insulin resistance on the other hand was confirmed by the decreased expression of key regulator genes of glucose uptake and use in muscle of androgen-deficient HFD-fed mice compared with controls. However, we show that muscle-specific AR deletion alone does not worsen the HFD-induced metabolic alterations. On the other hand, it has been shown that liver-specific (34) and adipocyte-specific (48) AR ablation are sufficient to exacerbate the HFD-induced adiposity and glucose intolerance.

In line with their increased fat mass and insulin resistance, HFD ORX mice displayed strongly decreased circulating levels of adiponectin. Obesity and T2D are associated with hypoadiponectinemia (49). The relation between androgen status and adiponectin levels is however less clear. Inverse association between serum androgen and adiponectin has been demonstrated both in mice

and humans (50, 51), which is not in agreement with our results, but not all studies concur. Indeed, 2 cross-sectional studies report a positive correlation between serum T and adiponectin (52, 53).

Insulin secretion in response to a glucose challenge was markedly reduced in both androgen-deficient models fed a HFD compared with the controls. In islets isolated from RD SHAM and RD ORX mice, which do not show metabolic alterations, glucose-stimulated insulin release was however similar, suggesting that the pancreatic β-cell failure observed in androgen-deficient HFD-fed animals is likely an indirect consequence of the peripheral insulin resistance. However, a direct effect of androgen deficiency in promoting insulin secretory defect cannot be totally excluded. Indeed, ex vivo stimulation of rat pancreatic islets with T leads to an increase in insulin secretion (54).

We investigated whether the above-mentioned metabolic effects of hypogonadism could be reversed by androgen replacement with T or DHT. Interestingly, the castration effects on body composition, serum leptin, glucose tolerance, and pancreatic insulin secretion were restored by T but not DHT supplementation. This confirms other studies in obese or diabetic mouse models demonstrating the importance of T aromatization. Indeed, male mice lacking the aromatase gene show increased adiposity, hyperglycemia, as well as insulin resistance (55, 56). Accordingly, treatment of castrated mice with combined T and aromatase inhibitor increased fat mass compared with T treatment alone (57). In men also, several lines of evidence underline the importance of aromatization for the effects of androgens on body composition and glucose homeostasis. A recent study for instance shows that T suppression in men increases fat mass due to loss of substrate for aromatization (40). Hence, aromatizable androgens are preferable if treatment of hypogonadal men with obesity and/or T2D is considered.

In summary, androgen deficiency per se has no deleterious effects on metabolic parameters, but potentiates HFD-induced metabolic alterations, including increased adiposity, impaired glucose tolerance, and decreased insulin secretion and sensitivity. When translated to humans, this indicates that endogenous hypogonadism as well as androgen deprivation therapy may accelerate the development of metabolic syndrome in men, although this may be avoided with a healthy diet. Our findings may have implications for the prevention of metabolic alterations in hypogonadal men.

Acknowledgments

We thank Rita Bollen, Hilde Debruyn, Dieter Schollaert, Erik Van Herck, Ludo Deboel, Riet Van Looveren, Karen Moermans, and Mikaela Granvik for their excellent technical assistance. We also thank Roman Vangoitsenhoven for his help with indirect calorimetry, Rodrigo Fernández-Verdejo for his help with citrate synthase activity measurements, and Geoffroy de Faudeur for his suggestions on the glucose tolerance tests and insulin measurements.

Address all correspondence and requests for reprints to: Frank Claessens, Molecular Endocrinology Laboratory, Department of Cellular and Molecular Medicine, KU Leuven, Campus Gasthuisberg O&N1 PO Box 901, Herestraat 49, 3000 Leuven, Belgium. E-mail: frank.claessens@med.kuleuven.be.

This work was supported by the KU Leuven Grant GOA/15/017 and the Research Foundation Flanders Grant G.0858.11.

Disclosure Summary: M.R.L. has consulted for Novartis and received lecture fees from Flanders' Agricultural Marketing Board, both unrelated to this work. V.D., M.R.L., and F.J. are fellows of the Research Foundation Flanders. All other authors have nothing to disclose.

References

1. **Ng M, Fleming T, Robinson M, et al.** Global, regional, and national prevalence of overweight and obesity in children and adults during 1980–2013: a systematic analysis for the Global Burden of Disease Study 2013. *Lancet*. 2014;384(9945):766–781.
2. **Alberti KG, Zimmet P, Shaw J.** Metabolic syndrome–a new worldwide definition. A consensus statement from the International Diabetes Federation. *Diabet Med*. 2006;23(5):469–480.
3. **Islam MS, Loots du T.** Experimental rodent models of type 2 diabetes: a review. *Methods Find Exp Clin Pharmacol*. 2009;31(4):249–261.
4. **Claessens F, Denayer S, Van Tilborgh N, Kerkhofs S, Helsen C, Haelens A.** Diverse roles of androgen receptor (AR) domains in AR-mediated signaling. *Nucl Recept Signal*. 2008;6:e008.
5. **Bhasin S, Pencina M, Jasuja GK, et al.** Reference ranges for testosterone in men generated using liquid chromatography tandem mass spectrometry in a community-based sample of healthy nonobese young men in the Framingham Heart Study and applied to three geographically distinct cohorts. *J Clin Endocrinol Metab*. 2011;96(8):2430–2439.
6. **Tajar A, Huhtaniemi IT, O'Neill TW, et al.** Characteristics of androgen deficiency in late-onset hypogonadism: results from the European Male Aging Study (EMAS). *J Clin Endocrinol Metab*. 2012;97(5):1508–1516.
7. **Grossmann M.** Low testosterone in men with type 2 diabetes: significance and treatment. *J Clin Endocrinol Metab*. 2011;96(8):2341–2353.
8. **Dhindsa S, Miller MG, McWhirter CL, et al.** Testosterone concentrations in diabetic and nondiabetic obese men. *Diabetes Care*. 2010;33(6):1186–1192.
9. **Ding EL, Song Y, Malik VS, Liu S.** Sex differences of endogenous sex hormones and risk of type 2 diabetes: a systematic review and meta-analysis. *JAMA*. 2006;295(11):1288–1299.
10. **Allan CA, Collins VR, Frydenberg M, McLachlan RI, Matthiesson KL.** Androgen deprivation therapy complications. *Endocr Relat Cancer*. 2014;21(4):T119–T129.
11. **Lin HY, Xu Q, Yeh S, Wang RS, Sparks JD, Chang C.** Insulin and leptin resistance with hyperleptinemia in mice lacking androgen receptor. *Diabetes*. 2005;54(6):1717–1725.
12. **De Gendt K, Swinnen JV, Saunders PT, et al.** A Sertoli cell-selective

knockout of the androgen receptor causes spermatogenic arrest in meiosis. *Proc Natl Acad Sci USA*. 2004;101(5):1327–1332.
13. **Dubois V, Laurent MR, Sinnesael M, et al.** A satellite cell-specific knockout of the androgen receptor reveals myostatin as a direct androgen target in skeletal muscle. *FASEB J*. 2014;28(7):2979–2994.
14. **Vandenput L, Boonen S, Van Herck E, Swinnen JV, Bouillon R, Vanderschueren D.** Evidence from the aged orchidectomized male rat model that 17β-estradiol is a more effective bone-sparing and anabolic agent than 5α-dihydrotestosterone. *J Bone Miner Res*. 2002;17(11):2080–2086.
15. **Vanderschueren D, Vandenput L, Boonen S, Van Herck E, Swinnen JV, Bouillon R.** An aged rat model of partial androgen deficiency: prevention of both loss of bone and lean body mass by low-dose androgen replacement. *Endocrinology*. 2000;141(5):1642–1647.
16. **Ferrannini E.** The theoretical bases of indirect calorimetry: a review. *Metabolism*. 1988;37(3):287–301.
17. **Okita K, Iwahashi H, Kozawa J, et al.** Homeostasis model assessment of insulin resistance for evaluating insulin sensitivity in patients with type 2 diabetes on insulin therapy. *Endocr J*. 2013;60(3):283–290.
18. **Friedewald WT, Levy RI, Fredrickson DS.** Estimation of the concentration of low-density lipoprotein cholesterol in plasma, without use of the preparative ultracentrifuge. *Clin Chem*. 1972;18(6):499–502.
19. **Verhaeghe J, van Herck E, Visser WJ, et al.** Bone and mineral metabolism in BB rats with long-term diabetes. Decreased bone turnover and osteoporosis. *Diabetes*. 1990;39(4):477–482.
20. **Lemaire K, Ravier MA, Schraenen A, et al.** Insulin crystallization depends on zinc transporter ZnT8 expression, but is not required for normal glucose homeostasis in mice. *Proc Natl Acad Sci USA*. 2009;106(35):14872–14877.
21. **Brouwers B, de Faudeur G, Osipovich AB, et al.** Impaired islet function in commonly used transgenic mouse lines due to human growth hormone minigene expression. *Cell Metab*. 2014;20(6):979–990.
22. **Lowry OH, Passonneau JV.** *A Flexible System of Enzymatic Analysis*. New York, NY: Academic Press; 1972.
23. **Essén-Gustavsson B, Henriksson J.** Enzyme levels in pools of microdissected human muscle fibres of identified type. Adaptive response to exercise. *Acta Physiol Scand*. 1984;120(4):505–515.
24. **Daval M, Diot-Dupuy F, Bazin R, et al.** Anti-lipolytic action of AMP-activated protein kinase in rodent adipocytes. *J Biol Chem*. 2005;280(26):25250–25257.
25. **De Pauw A, Tejerina S, Raes M, Keijer J, Arnould T.** Mitochondrial (dys)function in adipocyte (de)differentiation and systemic metabolic alterations. *Am J Pathol*. 2009;175(3):927–939.
26. **Heilbronn LK, Gan SK, Turner N, Campbell LV, Chisholm DJ.** Markers of mitochondrial biogenesis and metabolism are lower in overweight and obese insulin-resistant subjects. *J Clin Endocrinol Metab*. 2007;92(4):1467–1473.
27. **Tanti JF, Ceppo F, Jager J, Berthou F.** Implication of inflammatory signaling pathways in obesity-induced insulin resistance. *Front Endocrinol*. 2012;3:181.
28. **Fukui M, Kitagawa Y, Ose H, Hasegawa G, Yoshikawa T, Nakamura N.** Role of endogenous androgen against insulin resistance and athero- sclerosis in men with type 2 diabetes. *Curr Diabetes Rev*. 2007;3(1):25–31.
29. **Basaria S, Lieb J 2nd, Tang AM, et al.** Long-term effects of androgen deprivation therapy in prostate cancer patients. *Clin Endocrinol*. 2002;56(6):779–786.
30. **Marin P.** Testosterone and regional fat distribution. *Obesity Res*. 1995;3(suppl 4):609S–612S.
31. **Wu FC, Tajar A, Pye SR, et al.** Hypothalamic-pituitary-testicular axis disruptions in older men are differentially linked to age and modifiable risk factors: the European Male Aging Study. *J Clin Endocrinol Metab*. 2008;93(7):2737–2745.
32. **Rastrelli G, Carter EL, Ahern T, et al.** Development of and recovery from secondary hypogonadism in ageing men: prospective results from the EMAS. *J Clin Endocrinol Metab*. 2015;100(8):3172–3182.
33. **Hammoud A, Gibson M, Hunt SC, et al.** Effect of Roux-en-Y gastric bypass surgery on the sex steroids and quality of life in obese men. *J Clin Endocrinol Metab*. 2009;94(4):1329–1332.
34. **Lin HY, Yu IC, Wang RS, et al.** Increased hepatic steatosis and insulin resistance in mice lacking hepatic androgen receptor. *Hepatology*. 2008;47(6):1924–1935.
35. **Scheuner D, Vander Mierde D, et al.** Control of mRNA translation preserves endoplasmic reticulum function in β cells and maintains glucose homeostasis. *Nat Med*. 2005;11(7):757–764.
36. **Fan W, Yanase T, Nomura M, et al.** Androgen receptor null male mice develop late-onset obesity caused by decreased energy expenditure and lipolytic activity but show normal insulin sensitivity with high adiponectin secretion. *Diabetes*. 2005;54(4):1000–1008.
37. **Rana K, Fam BC, Clarke MV, Pang TP, Zajac JD, MacLean HE.** Increased adiposity in DNA binding-dependent androgen receptor knockout male mice associated with decreased voluntary activity and not insulin resistance. *Am J Physiol Endocrinol Metab*. 2011;301(5):E767–E778.
38. **Ophoff J, Callewaert F, Venken K, et al.** Physical activity in the androgen receptor knockout mouse: evidence for reversal of androgen deficiency on cancellous bone. *Biochem Biophys Res Commun*. 2009;378(1):139–144.
39. **Shi H, Seeley RJ, Clegg DJ.** Sexual differences in the control of energy homeostasis. *Front Neuroendocrinol*. 2009;30(3):396–404.
40. **Finkelstein JS, Lee H, Burnett-Bowie SA, et al.** Gonadal steroids and body composition, strength, and sexual function in men. *N Engl J Med*. 2013;369(11):1011–1022.
41. **Christoffersen B, Raun K, Svendsen O, Fledelius C, Golozoubova V.** Evalution of the castrated male Sprague-Dawley rat as a model of the metabolic syndrome and type 2 diabetes. *Int J Obes (Lond)*. 2006;30(8):1288–1297.
42. **Spalding KL, Arner E, Westermark PO, et al.** Dynamics of fat cell turnover in humans. *Nature*. 2008;453(7196):783–787.
43. **Ibebunjo C, Eash JK, Li C, Ma Q, Glass DJ.** Voluntary running, skeletal muscle gene expression, and signaling inversely regulated by orchidectomy and testosterone replacement. *Am J Physiol Endocrinol Metab*. 2011;300(2):E327–E340.
44. **Asarian L, Geary N.** Modulation of appetite by gonadal steroid hormones. *Philos Trans R Soc Lond B Biol Sci*. 2006;361(1471):1251–1263.
45. **Senmaru T, Fukui M, Okada H, et al.** Testosterone deficiency induces markedly decreased serum triglycerides, increased small dense LDL, and hepatic steatosis mediated by dysregulation of lipid assembly and secretion in mice fed a high-fat diet. *Metabolism*. 2013;62(6):851–860.
46. **Korenblat KM, Fabbrini E, Mohammed BS, Klein S.** Liver, muscle, and adipose tissue insulin action is directly related to intrahepatic triglyceride content in obese subjects. *Gastroenterology*. 2008;134(5):1369–1375.
47. **Ramamani A, Aruldhas MM, Govindarajulu P.** Differential response of rat skeletal muscle glycogen metabolism to testosterone and estradiol. *Can J Physiol Pharmacol*. 1999;77(4):300–304.
48. **McInnes KJ, Smith LB, Hunger NI, Saunders PT, Andrew R, Walker BR.** Deletion of the androgen receptor in adipose tissue in male mice elevates retinol binding protein 4 and reveals independent effects on visceral fat mass and on glucose homeostasis. *Diabetes*. 2012;61(5):1072–1081.
49. **Weyer C, Funahashi T, Tanaka S, et al.** Hypoadiponectinemia in obesity and type 2 diabetes: close association with insulin resistance and hyperinsulinemia. *J Clin Endocrinol Metab*. 2001;86(5):1930–1935.
50. **Nishizawa H, Shimomura I, Kishida K, et al.** Androgens decrease plasma adiponectin, an insulin-sensitizing adipocyte-derived protein. *Diabetes*. 2002;51(9):2734–2741.

51. **Lanfranco F, Zitzmann M, Simoni M, Nieschlag E.** Serum adiponectin levels in hypogonadal males: influence of testosterone replacement therapy. *Clin Endocrinol*. 2004;60(4):500–507.
52. **Isobe T, Saitoh S, Takagi S, et al.** Influence of gender, age and renal function on plasma adiponectin level: the Tanno and Sobetsu study. *Eur J Endocrinol*. 2005;153(1):91–98.
53. **Laughlin GA, Barrett-Connor E, May S.** Sex-specific association of the androgen to oestrogen ratio with adipocytokine levels in older adults: the Rancho Bernardo Study. *Clin Endocrinol*. 2006;65(4):506–513.
54. **Grillo ML, Jacobus AP, Scalco R, et al.** Testosterone rapidly stimulates insulin release from isolated pancreatic islets through a nongenomic dependent mechanism. *Horm Metab Res*. 2005;37(11):662–665.
55. **Takeda K, Toda K, Saibara T, et al.** Progressive development of insulin resistance phenotype in male mice with complete aromatase (CYP19) deficiency. *J Endocrinol*. 2003;176(2):237–246.
56. **Van Sinderen ML, Steinberg GR, Jorgensen SB, et al.** Hepatic glucose intolerance precedes hepatic steatosis in the male aromatase knockout (ArKO) mouse. *PLoS One*. 2014;9(2):e87230.
57. **Movérare-Skrtic S, Venken K, Andersson N, et al.** Dihydrotestosterone treatment results in obesity and altered lipid metabolism in orchidectomized mice. *Obesity*. 2006;14(4):662–672.